Charge and magnetization perturbations around impurities in nickel

N. Stefanou, A. Oswald, R. Zeller, and P. H. Dederichs
Institut für Festkörperforschung der Kernforschungsanlage, D-5170 Jülich, Federal Republic of Germany
(Received 22 October 1986)

We report about self-consistent calculations for dilute Ni alloys, which are based on density-functional theory and the Korringa-Kohn-Rostoker Green's-function method. In particular, we calculate the charge and magnetization perturbations for four shells of atoms around the impurity. Impurities of the 3*d*, 4*d*, and 4*sp* series are considered. Of central interest is the transition from strong to weak ferromagnetism and the different screening mechanism in these alloys. We compare our results for the perturbations of the local moments as well as the change of the total moment with magnetization and neutron scattering data.

I. INTRODUCTION

Ferromagnetic alloys of nickel, cobalt, and iron show a fascinating richness in their magnetic behavior. The total moment of the metal can either increase or decrease upon the addition of impurities. As far as the concentration dependence of the magnetization is concerned, concentrated alloys show normally a very similar behavior as dilute ones. By plotting the magnetization versus the electron-to-atom ratio the Slater-Pauling curve[1,2] brings a remarkable order into the experimental data. In the case of Ni-based alloys, *Ni*Co, *Ni*Fe, and dilute *Ni*Mn fall on the main branch of the Slater-Pauling curve and are, according to our present understanding, characterized by a filled majority *d* band ("strong ferromagnets"). On the other hand, Ni alloys with early transition-metal atoms such as *Ni*Cr, *Ni*V, etc., show pronounced deviations from the main branch of the Slater-Pauling curve which are due to emptying of the majority band ("weak ferromagnets").

The work of Friedel,[3] Kanamori,[4] and Campbell and Gomes[5] has lead to a basic understanding of the magnetic behavior of these alloys. The essential point is that for strong ferromagnets the majority band is full so that the integrated density of states $N^{\uparrow}(E_F)$ for majority spin does not change due to the addition of an impurity, i.e., $\Delta N^{\uparrow}(E_F)=0$. If ΔZ is the difference between impurity and host atomic numbers, the total neutrality condition $\Delta N^{\uparrow}(E_F)+\Delta N^{\downarrow}(E_F)=\Delta Z$ implies that the moment of the alloy changes for each impurity by

$$\Delta M=\Delta N^{\uparrow}(E_F)-\Delta N^{\downarrow}(E_F)=-\Delta Z \ .$$

On the other hand, for the early transition-metal impurities, an empty impurity *d* state is located in the majority band above the Fermi energy, so that $\Delta N^{\uparrow}(E_F)=-5$. Consequently, the moment changes by $\Delta M=-10-\Delta Z$. Clearly these arguments are based on a tight-binding model. Owing to the developments of density-functional theory and sophisticated numerical techniques we are now able to perform realistic *ab initio* calculations and we are in a position to check the reliability of such models.

The case of dilute Ni and Co alloys is especially complicated, since a long-range magnetization perturbation exists around the early 3*d* impurities, as has been found in neutron scattering experiments.[6] This necessarily asks for self-consistently calculating the charge and magnetization disturbance of a large number of atoms around the impurity. Owing to the development of the Korringa-Kohn-Rostoker (KKR) Green's-function method, such large-scale calculations have become feasible recently. This is also important from another point of view. As has been pointed out by Williams *et al.*[7,8] the above arguments are based on the Friedel sum rules for charge and magnetization, i.e., on state counting. Thus it needs a very accurate summation of the charge and magnetization density in the whole space in order to calculate these quantities. Unfortunately any argument based on local bonding and hybridization is in danger of missing the simplicity[7,9,10] brought about by these sum rules.

For metalloid impurities like Cu, Zn, Ga, ... the experiments show that the change of the total moment decreases with the valence of the impurity,[11,12] i.e., $\Delta M=-\Delta Z$, and that the range of the magnetization perturbation is similar to that of the early 3*d* impurities. This behavior was originally understood on a rigid-band basis,[12] with the *sp* impurities giving away their valence electrons in order to fill up the minority host band. However, this process is quite unrealistic since it requires enormous charge transfer. Friedel[3] and especially Terakura and Kanamori[13] have shown that the *sp* impurities are well screened locally by a state-conserving mechanism and that the additional states required to achieve neutrality are gained by filling up the minority *d* band. In this context it is most important that the hybridization between the impurity *sp* states and the Ni *d* states leads to a hybridization minimum in the impurity density of states close to the Fermi energy, thus clearly separating the lower lying and occupied bonding states from the higher antibonding ones which are not populated. However, this holds only for the early *sp* impurities. For more attractive impurities new *sp* states are added below the Fermi energy and provide the screening which leads to the transition to weak ferromagnetism. Williams *et al.*[7,8] have recently pointed out the importance and generality of these two different screening processes for understanding ferromagnetic metalloid alloys. Our paper is aimed at elucidating

these mechanisms with present state-of-the-art methods and to study the transition from d-state screening to sp-state screening for third-row impurities. The present paper completes two recent theoretical studies of dilute Ni alloys. Zeller[14] has calculated the local moments of $3d$ and $4d$ impurities, whereas Blügel *et al.*[15] have given a detailed discussion of the hyperfine fields.

II. THEORETICAL METHOD

Our calculational method is based on multiple scattering theory using the KKR Green's-function scheme. For a lattice of muffin-tin potentials centered at positions $\mathbf{R}^n$, the Green's function can be expanded into eigensolutions of these spherically symmetric local potentials[16,17]

$$G(\mathbf{r}+\mathbf{R}^n,\mathbf{r}'+\mathbf{R}^{n'};E)=-i\sqrt{E}\,\delta_{nn'}\sum_L Y_L(\hat{\mathbf{r}})R_l^n(r_<,E)H_l^n(r_>,E)Y_L(\hat{\mathbf{r}}')+\sum_{L,L'} Y_L(\hat{\mathbf{r}})R_l^n(r,E)G_{LL'}^{nn'}(E)R_{l'}^{n'}(r',E)Y_{L'}(\hat{\mathbf{r}}')\ , \quad (1)$$

in Rydberg atomic units. The position vectors $\mathbf{r},\mathbf{r}'$ are restricted to the Wigner-Seitz cell and $r_<,r_>$ are the smaller and larger of $r=|\mathbf{r}|$ and $r'=|\mathbf{r}'|$. The subscript $L=(l,m)$ denotes angular-momentum quantum numbers and Y_L are real spherical harmonics. The irregular H_l^n and regular R_l^n solutions of the radial Schrödinger equation for the nth muffin-tin potential at an energy E are defined by their asymptotic behavior outside the muffin-tin sphere of radius $R_{\rm MT}$:

$$\begin{aligned} H_l^n(r,E)&=h_l(r\sqrt{E})\ ,\\ R_l^n(r,E)&=j_l(r\sqrt{E})-i\sqrt{E}\,t_l^n(E)h_l(r\sqrt{E}),\quad r>R_{\rm MT}\end{aligned} \quad (2)$$

where j_l,h_l are the spherical Bessel and Hankel functions and t_l^n is the usual t matrix for the nth single potential.

The information about the multiple scattering between muffin tins is contained in the structural Green's-function matrix $G_{LL'}^{nn'}$. It can be related to its counterpart for the host crystal by an algebraic Dyson equation:

$$G_{LL'}^{nn'}(E)=G_{LL'}^{0nn'}(E)+\sum_{n'',L''}G_{LL''}^{0nn''}(E)[t_{l''}^{n''}(E)-t_{l''}^{0n''}(E)]G_{L''L'}^{n''n'}(E)\ , \quad (3)$$

where the 0 superscript refers to the host. This equation describes correctly and in a very efficient way the embedding of the defect into the ideal crystal. In our calculation the angular-momentum expansion in the Green's functions includes s, p, and d electrons. The potentials on the impurity [(000) site], the 12 first Ni nearest neighbors [(110) shell], the 6 second Ni nearest neighbors [(200) shell], the 24 third Ni nearest neighbors [(210) shell], and the 12 fourth Ni nearest neighbors [(220) shell] are allowed to respond self-consistently to the perturbation induced by the impurity. The resulting 495×495 matrix equation (3) is solved using group-theoretical methods.[17] In this way the problem is reduced to the inversion of smaller submatrices, the maximal size of which is 37×37. The one-electron effective potentials of the 55-atom perturbed cluster are determined self-consistently in the framework of density-functional theory. Exchange and correlation effects are included through the local spin-density approximation of von Barth and Hedin with the constants as given by Moruzzi *et al.*[18]

The necessary charge density is obtained for the valence states by complex energy integration of the Green's function up to the host Fermi level E_F using 64 complex energies z:[19]

$$\rho_v^\sigma(\mathbf{r}+\mathbf{R}^n)=-\frac{1}{\pi}\,\mathrm{Im}\oint dz G^\sigma(\mathbf{r}+\mathbf{R}^n,\mathbf{r}+\mathbf{R}^n;z) \quad (4)$$

and by considering the core states as frozen. Here, the index σ stands for spin direction, allowing thus for spin polarization. The use of an improved iteration scheme[20] accelerates considerably the convergence of the self-consistency iterations. The charge and magnetization distributions around the impurity are calculated directly from the spin densities:

$$\delta Q^n=\int_{n\text{th cell}} d\mathbf{r}[\rho^\uparrow(\mathbf{r}+\mathbf{R}^n)+\rho^\downarrow(\mathbf{r}+\mathbf{R}^n)]\ , \quad (5)$$

$$\delta M^n=\int_{n\text{th cell}} d\mathbf{r}[\rho^\uparrow(\mathbf{r}+\mathbf{R}^n)-\rho^\downarrow(\mathbf{r}+\mathbf{R}^n)]\ , \quad (6)$$

approximating the Wigner-Seitz cell by the atomic sphere. On the other hand, the total displaced charge ΔQ is given by the change $\Delta N(E_F)$ of the integrated density of states at the Fermi energy:

$$\Delta Q=\Delta N(E_F)=\Delta N^\uparrow(E_F)+\Delta N^\downarrow(E_F)\ , \quad (7)$$

which can be calculated by Lehmann's adaptation of Lloyd's formula.[21]

$$\Delta N^\sigma(E)=-\frac{1}{\pi}\,\mathrm{Im\,Tr\,ln}\{[(t-t^0)^{-1}-G^0]t^0t^{0\dagger-1}\}_{(E)}^\sigma\ . \quad (8)$$

Analogously, the change of the total moment ΔM induced by the impurity is given by:

$$\Delta M=\Delta N^\uparrow(E_F)-\Delta N^\downarrow(E_F)\ . \quad (9)$$

Ideally, if all the perturbed potentials could be taken into account in the self-consistent calculation, the total displaced charge, as well as the charge perturbation summed over all the perturbed atoms, would satisfy exactly the Friedel's screening rule, which expresses the total neutrality of the crystal:

$$\Delta Q=\sum_{n\in\text{cluster}}\Delta Q^n=\Delta N(E_F)=\Delta Z\ , \quad (10)$$

ΔZ being the difference between impurity and host atomic numbers. An equivalent sum rule also holds for the magnetization perturbation:

$$\Delta M=\sum_{n\in\text{cluster}}\delta M^n=\left[\frac{dM}{dC}\right]_{c\to0}\ , \quad (11)$$

where $(dM/dc)_{c\to 0}$ is the experimental change of saturation spin magnetization $M(c)$ in the dilute limit of zero concentration c.

Since only potentials up to the fourth shell around the impurity are allowed to be perturbed, equations (10) and (11) are not satisfied exactly in our calculation. The deviation of the calculated screening charge from the ideal value ΔZ gives an indication of the error involved and of the importance of including more perturbed shells. This point is investigated in more detail in Sec. III B.

III. RESULTS AND DISCUSSION

A. 3d impurities in Ni

Table I lists the calculated charge and magnetization perturbation around $3d$ and $4sp$ impurities in Ni, i.e., all impurities of the third row of the periodic table. ΔQ^0 denotes the difference between the charge in the impurity Wigner-Seitz sphere and the corresponding charge in pure Ni. The quantities ΔQ^n, $n=1,\ldots,4$ denote the charge changes in the nth shell around the impurity, i.e., the charge of a Ni atom in the nth shell multiplied with the number of Ni atoms per shell, e.g., 12 for $n=1$. $\Delta Q^{\rm cl}=\Delta Q^1+\Delta Q^2+\cdots+\Delta Q^4$ is the total change of the charge in the cluster of 55 atoms. This should be compared with ΔQ which has been calculated by using equations (7) and (8) and the self-consistent t matrices for four shells. $M^{\rm imp}$ is the impurity moment and δM^n the change of the moment of a Ni atom in the nth shell. These quantities refer to the corresponding Wigner-Seitz spheres of the atoms. $\Delta M^{\rm cl}$ is the change of the moment in the cluster of 55 atoms and ΔM is the total change of the moment in the whole crystal as calculated by the Eqs. (8) and (9).

The close agreement between the quantities ΔQ and ΔM calculated by the Friedel sum and the changes $\Delta Q^{\rm cl}$ and $\Delta M^{\rm cl}$ inside the cluster indicate that in a good approximation the perturbation is localized within the first four shells around the impurities. Exceptions are K and Br impurities, where the differences between ΔQ and $\Delta Q^{\rm cl}$, ΔM and $\Delta M^{\rm cl}$, respectively, seem to indicate even longer-ranged perturbations.

We shall discuss in the paragraph our results for the $3d$ impurities, whereas the results for sp impurities will be analyzed in Sec. III D. For Co impurities the local moment is about $1\mu_B$ larger than the Ni moment, for Fe impurities it is about $2\mu_B$ larger. In both cases there is nearly no charge and especially no magnetization disturbance on the neighboring shells. Therefore the change ΔM of the total moment (see Fig. 1) is determined by the impurity moment alone, so that approximately $\Delta M\cong 1$ for Co and $\Delta M\cong 2$ for Fe impurities. The physical reason for this simple behavior is that the majority band is full, both in pure Ni and in the *Ni*Co and *Ni*Fe alloys. Figure 2 shows the integrated densities of states at E_F for both spin directions. It is seen that for Co and Fe and to some minor degree also for Mn there is no change in the majority band population $[\Delta N^{\uparrow}(E_F)\approx 0]$, so that the change ΔM arises alone from the negative change of $\Delta N^{\downarrow}(E_F)$ which due to charge neutrality results into $\Delta M\cong=-\Delta Z$.

As an example of these strong ferromagnets we show in Fig. 3 the local density of states (LDOS) of an Fe impurity. The majority band has practically the same shape and position as the Ni majority band. The same is also true for Co impurities[14] and is the result of two counteracting effects. Compared to pure Ni, the electrostatic potential on the Fe site is weakened which is however compensated in the majority band by the increased exchange attraction

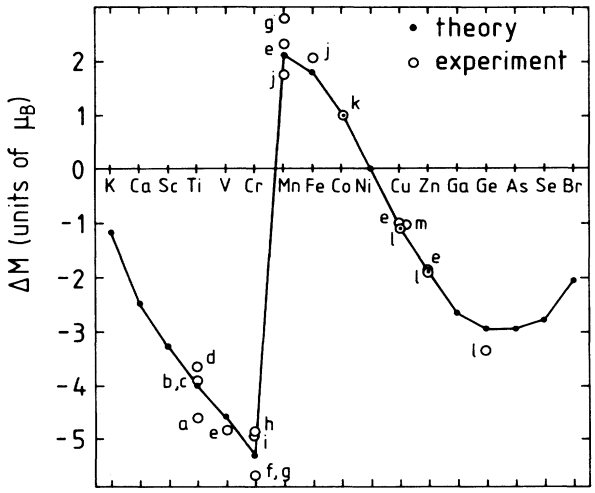

FIG. 1. Change $\Delta M=(dM/dc)\,|_{c=0}$ of the magnetization of dilute Ni alloys with third-row elements. The experimental data are corrected for orbital contributions (see text), so that only spin moments are compared. The references to the experimental data (○) are: (a) F. Kajzar and G. Parette, Phys. Rev. B **20**, 2002 (1979); (b) I. P. Gregory and D. E. Moody, J. Phys. F **5**, 36 (1975); (c) W. S. Chan, K. Mitsuoka, H. Miyajima, and S. Chikazumi, J. Phys. Soc. Jpn. **48**, 822 (1980); (d) V. Marian, Ann. Phys. (Paris) **7**, 459 (1937); (e) Ref. 11; (f) Ref. 25; (g) H. C. Van Elst, B. Lubach, and G. J. Van den Berg, Physica **28**, 1297 (1962); (h) M. J. Besnus, Y. Gottehrer, and G. Munschy, Phys. Status Solidi B **49**, 597 (1972); (i) R. Chiffey and T. J. Hicks, Phys. Lett. **34 A**, 267 (1971); (j) M. F. Collins and G. G. Low, Proc. Phys. Soc. London **86**, 535 (1965); (k) Refs. 1 and 2; (l) Ref. 12; (m) Ref. 26.

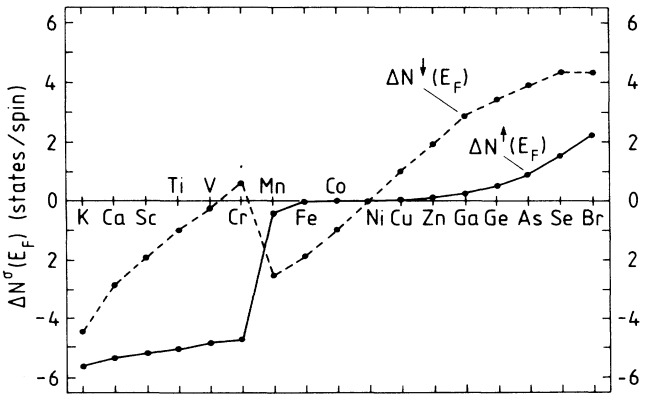

FIG. 2. Changes $\Delta N^{\uparrow}(E_F)$ and $\Delta N^{\downarrow}(E_F)$ of the majority and minority band populations for third-row impurities in Ni.

TABLE I. Charge and magnetization perturbations around third-row impurities in Ni. ΔQ^0: change of charge in the impurity Wigner-Seitz sphere with respect to pure Ni; ΔQ^n: change of the total charge in the nth shell around the impurity, $\Delta Q^{cl}=\Delta Q^0+\Delta Q^1+\Delta Q^2+\Delta Q^3+\Delta Q^4$; ΔQ: change of total charge as calculated by Friedel's sum rule (8); M^{imp}: local moment of the impurity; δM^n: change of the local moment of an atom in the nth shell; ΔM^{cl}: change of the moment in the cluster of 55 atoms; ΔM: change of the moment as calculated by Friedel's sum rule (8).

	K	Ca	Sc	Ti	V	Cr	Mn	FE	Co	Ni	Cu	Zn	Ga	Ge	As	Se	Br
ΔQ^0	−8.888	−8.599	−7.877	−6.817	−5.666	−4.478	−3.376	−2.265	−1.119	0	1.026	1.858	2.684	3.637	4.693	5.810	6.934
ΔQ^1	0.000	0.752	1.027	0.932	0.750	0.537	0.424	0.288	0.124	0	−0.016	0.187	0.414	0.485	0.452	0.361	0.241
ΔQ^2	0.106	0.071	0.047	0.026	0.012	0.008	−0.002	0.001	0.001	0	0.003	0.007	0.008	−0.001	−0.000	0.016	0.033
ΔQ^3	−0.148	−0.164	−0.146	−0.109	−0.081	−0.060	−0.041	−0.027	−0.013	0	−0.001	−0.030	−0.051	−0.094	−0.117	−0.117	−0.137
ΔQ^4	−0.080	−0.065	−0.054	−0.032	−0.013	−0.006	−0.004	0.004	0.009	0	−0.012	−0.022	−0.064	−0.029	−0.028	−0.084	−0.085
ΔQ^{cl}	−9.010	−8.005	−7.003	−6.000	−4.998	−3.999	−2.999	−1.999	−0.999	0	1.000	2.000	2.991	3.999	5.000	5.986	6.986
ΔQ	−9.898	−8.135	−7.069	−6.035	−5.008	−4.031	−2.923	−1.937	−0.957	0	0.999	2.025	3.166	3.972	4.831	5.867	6.567
								μ_B per atom									
M^{imp}	−0.014	−0.067	−0.133	−0.272	−0.562	−1.700	3.018	2.703	1.702	0.583	−0.013	−0.052	−0.052	−0.040	−0.014	0.029	0.075
δM^0	−0.598	−0.650	−0.717	−0.856	−1.145	−2.283	2.434	2.119	1.119	0	−0.596	−0.635	−0.636	−0.623	−0.598	−0.554	−0.508
δM^1	−0.034	−0.124	−0.164	−0.193	−0.204	−0.180	−0.033	−0.011	0.004	0	−0.033	−0.080	−0.126	−0.157	−0.163	−0.143	−0.099
δM^2	−0.011	−0.035	−0.042	−0.047	−0.046	−0.048	0.024	0.003	−0.003	0	−0.005	−0.016	−0.024	−0.028	−0.031	−0.033	−0.028
δM^3	−0.004	−0.007	−0.012	−0.017	−0.020	−0.018	0.002	0.001	0.002	0	−0.004	−0.006	−0.011	−0.008	−0.006	−0.007	−0.000
δM^4	−0.007	−0.000	−0.006	−0.012	−0.017	−0.012	−0.011	−0.014	−0.010	0	0.000	−0.006	−0.024	−0.014	−0.014	−0.032	−0.030
								μ_B									
ΔM^{cl}	−1.256	−2.528	−3.299	−4.013	−4.546	−5.300	2.109	1.862	1.067	0	−1.119	−1.915	−2.849	−3.027	−3.051	−3.019	−2.238
ΔM	−1.169	−2.484	−3.257	−3.988	−4.557	−5.319	2.140	1.813	1.017	0	−1.068	−1.871	−2.674	−2.935	−2.956	−2.791	−2.046

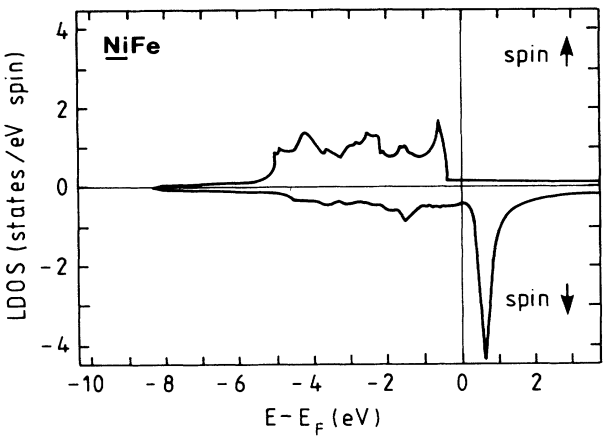

FIG. 3. LDOS for both spin directions of an Fe impurity in Ni.

since the local moment is larger by $2\mu_B$. Contrary to the minority band both effects superimpose on each other, expelling intensity into a sharp d peak to higher energies. Thus the screening is only performed by the minority electrons. Moreover, it is well localized in the impurity cell. Figure 4 shows the changes $\Delta N^{cl}(E)$ of the LDOS summed over all 55 atoms in the first 4 shells. The dashed line represents the change $\Delta N(E)$ of the integrated density of states, as obtained by the Friedel sum rule. For the majority band the changes in the band are small and canceling each other, so that $\Delta N^{\uparrow} \simeq 0$ at the upper band edge. Contrary to the minority band we just lose the missing two electrons in the region below E_F, so that $\Delta N^{\downarrow}(E_F) \cong -2$.

Mn impurities are an intermediate case. This is due to the fact that the Mn moment is not $3.7\mu_B$, as needed for strong ferromagnetism, but according to our results only about $3\mu_B$. In this case a virtual bound state develops in the energy region between the maximum of the majority band the the Fermi energy.[14] A small high-energy tail of this state is unoccupied, causing a slight drop in the occupation of the majority band [$\Delta N^{\uparrow}(E_F) = -0.39$, Fig. 2]. Connected with the deviation from strong ferromagnetism is an increasing polarization of the neighboring Ni atoms. Thus dilute *Ni*Mn is at the border of being a strong ferromagnet and concentrated Ni-Mn alloys show a complex behavior[1] with a tendency towards weak ferromagnetism. This is plausible from our results since the narrow peak is expected to broaden with concentration thus decreasing $\Delta N^{\uparrow}(E_F)$. The early transition-metal impurities (Cr, V, Ti, . . .) all show a virtual bound state in the majority band well above E_F. Therefore about five electrons are missing in the band [see Fig. 2, $\Delta N^{\uparrow}(E_F) \cong -5$] and the change ΔM of the total moment approximately follows the rule

$$\Delta M = \Delta N^{\uparrow}(E_F) - \Delta N^{\downarrow}(E_F) \cong -10 - \Delta Z$$

(see Fig. 1), since $\Delta Z = \Delta N^{\uparrow}(E_F) + \Delta N^{\downarrow}(E_F)$. Together with the change of sign of ΔM also the impurity moment changes sign and couples antiferromagnetically to the host moments. However the impurity moments are in general rather small and by far the largest contribution to ΔM comes from a strong reduction of the host moments in the four shells around the impurity. For instance, for V we have a local moment of $=0.56\mu_B$, giving only a contribution of $-1.15\mu_B$ from the impurity cell to the total change of $\Delta M = -4.55\mu_B$. The biggest contribution comes from the nearest neighbors which all together yield $-2.45\mu_B$. Note that the changes δM^n of the first four shells are negative and not oscillatory.

As a representative example for the early $3d$ impurities we will consider *Ni*V in more detail. Figure 5 shows the LDOS of the V impurity. For both spin directions we ob-

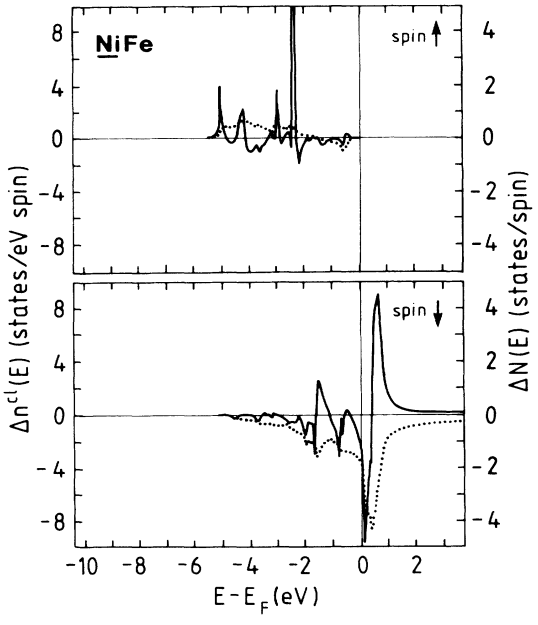

FIG. 4. Change $\Delta n^{cl}(E)$ of the density of states within the 55-atom cluster (solid line) and integrated total change $\Delta N(E)$ in the whole crystal (dotted line) for an Fe impurity in Ni.

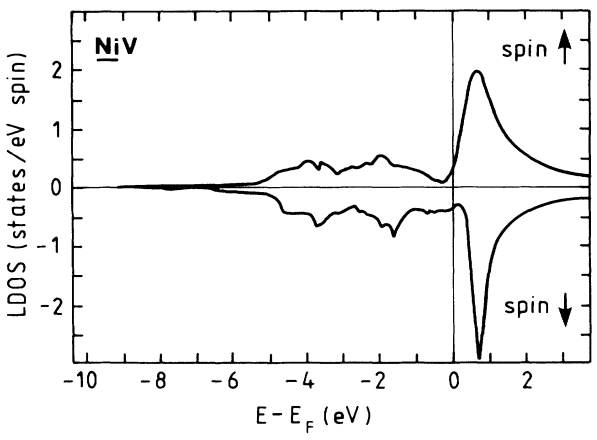

FIG. 5. LDOS of a V impurity in Ni.

tain pronounced virtual bound states above E_F which are located at about the same energy. The intensity within the minority band region is higher, indicating that the local moment is negative. Figure 6 shows the changes $\Delta N^{cl}(E)$ of the density of states of the 55-atom cluster (solid lines) and the changes of the integrated density of states $\Delta N(E)$.

In the majority band we have a more or less homogeneous loss of intensity in the whole band region which results in $\Delta N^{\uparrow}(E_F) = -4.8$ states which are transferred into the resonance above E_F. Contrary for the minority band there are practically no changes below E_F. Since $\Delta Z = -5$ only a very small change of the population, $\Delta N^{\downarrow}(E_F) = -0.2$, occurs in the minority band. Here large changes only occur above E_F, where intensity is transferred from the band edge to the resonance. For Ti and Sc this is no longer true, since $\Delta N^{\uparrow}(E_F)$ is nearly fixed at the value -5 so that the screening has to be accomplished by decreasing the population of the occupied states in the minority band.

The name "virtual bound state" for the empty impurity peaks in Fig. 5 might be somewhat misleading, since there is a very strong hybridization between the d states of the impurity and those of the host. In fact these peaks represent just the antibonding d-d hybrids while the corresponding bonding ones fall into the region of the Ni d band. Both type of states are clearly separated by a minimum in the LDOS close to E_F. Since the virtual bound states are energetically inaccessible, charge neutrality can in general only be achieved by filling up the minority band, leading to the simple behavior $\Delta M \cong -10 - \Delta Z$ for the moment. Thus the impurity is only screened by bonding hybrids, which results into a small charge transfer to the Ni neighbors. From Figs. 1 and 2 we see that the simple tight-binding model predicting $\Delta N^{\uparrow}(E_F) \cong -5$, $\Delta N^{\downarrow}(E_F) = 5 + \Delta Z$, and $\Delta M = -10 - \Delta Z$ gives a rather good global description of the behavior of the early transition-metal impurities. Nevertheless there are small deviations which are mostly due to two effects. Firstly, the virtual bound state in the majority band is not completely empty since a small tail extends in the region below the Fermi energy (see Fig. 5). Of course in a tight-binding model the width of the virtual bound state would be infinitely sharp thus fixing $\Delta N^{\uparrow}(E_F) = -5$. Even more important is that the number of s and p electrons changes slowly in the $3d$ series. For instance, locally the V impurity has 0.42 sp electrons less than pure Ni. As a consequence the change $\Delta N^{\uparrow}(E_F)$ in the majority band decreases for the early transition impurities and especially for Ca and K below the value -5. Since $\Delta M = 2\Delta N^{\uparrow}(E_F) - \Delta Z$ the moment ΔM therefore decreases even below the value $-10 - \Delta Z$. Figures 1 and 2 show that in the $3d$ series the transition from strong to weak ferromagnetism is rather sharp. Zeller has shown[14] that the situation is even more complicated. For instance for Mn two solutions are found, one with a positive moment corresponding to the values shown in Figs. 1 and 2 and Table I and a second "antiferromagnetic" solution with a negative moment similar to the Cr case. The latter is presumably metastable. In Fig. 1, together with the calculated changes ΔM of the total moment, we have also reported the available experimental data. The experimental values have been corrected for the orbital contribution so that only spin moments are compared. The part of the change of total magnetization which is localized on the impurity is corrected using the experimental g factor of the impurity atom in its elemental state when available [2.08 for Fe, 2.17 for Co (Ref. 22), otherwise we assume a g value of 2. For the remaining part of the total magnetization change, coming from the neighboring Ni shells, we have used the g factor of the elemental Ni [(2.19) of Ref. 22].

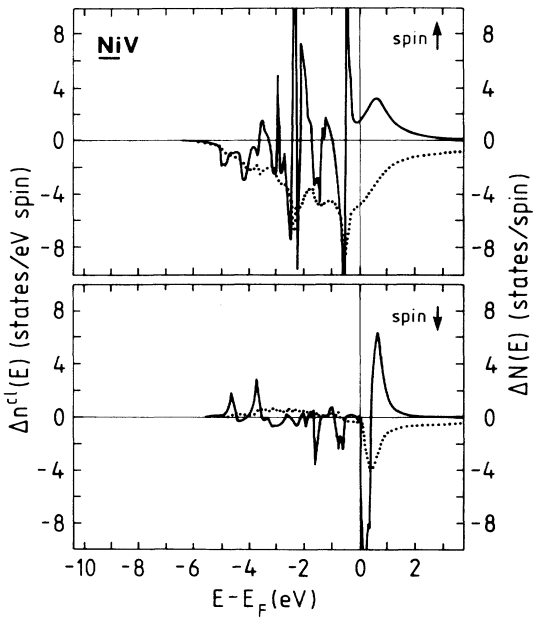

FIG. 6. Change $\Delta n^{cl}(E)$ within the 55-atom cluster (solid line) and change $\Delta N(E)$ of integrated density of states in the crystal (dotted line) for a V impurity in Ni.

In the case of *Ni*Fe and *Ni*Co alloys the magnetic perturbation is almost localized on the impurity whereas in *Ni*Mn the calculated small reduction of the first-neighboring Ni moment by $0.033\mu_B$ per atom is in good agreement with the experimental values of $0.028 \pm 0.007\mu_B$ per atom at 1.9% Mn and $0.007 \pm 0.018\mu_B$ per atom 1% Mn.[23] In the case of the early transition-metal impurities the magnetic perturbation is rather extended. The calculated large reductions of the first-neighboring Ni moment of $0.193\mu_B$ per atom in *Ni*Ti, $0.204\mu_B$ per atom in *Ni*V, and 0.180 per atom in *Ni*Cr agree quite well with neutron scattering data: $0.173 \pm 0.004\mu_B$ per atom,[24] $0.12 \pm 0.01\mu_B$ per atom,[25] and $0.20 \pm 0.01\mu_B$ per atom,[25] respectively. The moment is also reduced on the next neighboring Ni atoms which also agrees with the results of experimental measurements.[25] Comparison of the calculated local impurity moments with the experimental data is discussed elsewhere[14] and therefore will be not analyzed here.

B. Convergence as a function of the perturbed cluster size

We study here the convergence of our results as a function of the size of the perturbed cluster taken into account

TABLE II. Evolution and convergence of physical properties of *Ni*V as a function of the perturbed cluster size (same nomenclature as Table I).

	1-atom cluster	13-atom cluster	19-atom cluster	43-atom cluster	55-atom cluster
ΔQ^0	−5.400	−5.664	−5.665	−5.666	−5.666
ΔQ^1	−0.710[a]	0.705	0.714	0.749	0.750
ΔQ^2	−0.078[a]	0.055[a]	−0.017	0.012	0.012
ΔQ^3	−0.177[a]	0.070[a]	0.083[a]	−0.093	−0.081
ΔQ^4	0.272[a]	0.378[a]	0.383[a]	0.391[a]	−0.013
ΔQ^{cl}	−6.093	−4.456	−4.502	−4.607	−4.998
ΔQ	−6.107	−4.474	−4.504	−4.706	−5.008
			μ_B per atom		
δM^0	−1.275	−1.146	−1.148	−1.145	−1.145
δM^1	−0.051[a]	−0.202	−0.204	−0.205	−0.204
δM^2	−0.005[a]	−0.030[a]	−0.044	−0.048	−0.046
δM^3	−0.007[a]	−0.016[a]	−0.016[a]	−0.021	−0.020
δM^4	−0.022[a]	−0.031[a]	−0.031[a]	−0.031[a]	−0.017
			μ_B		
ΔM^{cl}	−2.359	−4.503	−4.610	−4.759	−4.546
ΔM	−2.578	−4.641	−4.746	−4.736	−4.557

[a]Non-self-consistent estimation.

in the self-consistency loop. For this purpose we have performed five different self-consistent calculations: a single site one, as well as "cluster calculations" including, in addition to the impurity 1, 2, 3, and 4 neighboring shells in the self-consistency process. Thus, the considered perturbed clusters contain 1, 13, 19, 43, and 55 atoms, respectively. The numerical investigation is performed for the *Ni*V alloy, where the perturbation is long ranged so that the differences between calculations with clusters of different size will be more pronounced. The results are listed in Table II. For each case, in addition to the results of self-consistent calculations for the charge and magnetic moment perturbation within the considered cluster, we report also a non-self-consistent estimation of the perturbation outside it, up to the fourth neighboring shell, i.e., our largest considered cluster. The non-self-consistent estimation is performed using unperturbed host potentials for the atoms outside the considered cluster, but self-consistent ones inside.

As it is clearly shown in Table II our self-consistency procedure favors cluster neutrality, whereas the Friedel's screening rule is progressively attained as additional shells

TABLE III. Charge and magnetization perturbation around 4*d* impurities in Ni (same nomenclature as in Table I).

	Y	Zr	Nb	Mo	Tc	Ru	Rh	Pd	Ag	Cd
ΔQ^0	9.721	10.574	11.659	12.830	14.025	15.268	16.444	17.564	18.520	19.300
ΔQ^1	1.556	1.674	1.547	1.340	1.120	0.842	0.640	0.512	0.567	0.838
ΔQ^2	0.090	0.065	0.043	0.027	0.012	0.003	0.010	0.017	0.026	0.030
ΔQ^3	−0.283	−0.244	−0.200	−0.166	−0.141	−0.110	−0.090	−0.076	−0.086	−0.119
ΔQ^4	−0.093	−0.075	−0.052	−0.032	−0.017	−0.005	−0.006	−0.020	−0.040	−0.053
ΔQ^{cl}	10.991	11.994	12.997	13.999	14.999	15.998	16.998	17.997	18.996	19.996
ΔQ	10.778	11.841	12.882	13.903	14.970	15.978	16.941	18.043	18.899	19.911
					μ_B per atom					
M^{imp}	−0.080	−0.138	−0.207	−0.247	−0.041	0.661	0.571	0.199	−0.013	−0.045
δM^0	−0.663	−0.722	−0.790	−0.831	−0.625	0.077	−0.012	−0.384	−0.597	−0.629
δM^1	−0.201	−0.236	−0.264	−0.276	−0.227	−0.066	−0.011	−0.011	−0.051	−0.102
δM^2	−0.051	−0.057	−0.059	−0.050	−0.008	0.040	0.022	0.007	−0.007	−0.018
δM^3	−0.008	−0.015	−0.020	−0.023	−0.016	0.005	0.007	0.004	−0.001	−0.004
δM^4	−0.001	−0.007	−0.013	−0.018	−0.017	−0.009	−0.004	0.004	0.004	−0.002
					μ_B					
ΔM^{cl}	−3.596	−4.322	−4.957	−5.207	−3.980	−0.471	0.120	−0.330	−1.219	−2.070
ΔM	−3.493	−4.238	−4.899	−5.161	−3.927	−0.346	0.191	−0.389	−1.117	−1.951

are taken into account in the self-consistent calculation. However, the important point is that the local quantities (charges or moments) calculated self-consistently are very stable as a function of the perturbed cluster size.

Even a single-site calculation gives a reasonable description both for the charge and magnetization of the impurity. These values are practically completely converged, if in addition to the impurity also the first shell is calculated self-consistently. Analogously the results for the first shell change only very little, if more shells are included in the self-consistency procedure. Table II shows that in general all local quantities are reliable once they are calculated self-consistently.

This is however not true for the non-self-consistent values. For instance the change of the charge on the first shell changes from -0.71 in a single-site calculation to the final value of $+0.75$, whereas the moment δM^1 of a first shell atom changes from $-0.051\mu_B$ to $-0.204\mu_B$. Thus non-self-consistently calculated values cannot be considered as reliable. The disagreement is however somewhat smaller for the moments than for the charges.

In this context it is interesting that charge and moment perturbations $\Delta Q^{\rm cl}$ and $\Delta M^{\rm cl}$ summed up over the 55-atom cluster agree very well with the total changes ΔQ and ΔM obtained by summing over the whole crystal through Eqs. (7)–(9). From this we conclude that the perturbation is fairly well localized within the 4-shell cluster.

C. 4*d* impurities in Ni

In Table III the numerical results for the 4*d* impurities are given. The nomenclature is the same as in Table I. The most important results are shown in Fig. 7, i.e., the change of the number of electrons in both subbands as calculated by the Friedel sums and the change ΔM of the moment.

Physically the most important difference between 4*d* and 3*d* impurities is the somewhat larger spatial extent of the 4*d* wave function, which leads to a stronger hybridization with the host and to a slightly smaller exchange integral. Since both are unfavorable for magnetism, 4*d* impurities are normally not magnetic in paramagnetic hosts such as Cu, Ag, or Pd. However in ferromagnets such as Ni the host magnetization induces local moments. In analogy to the 3*d* series the moment changes sign in the middle of the 4*d* series, i.e., we obtain positive moments for Pd, Rh, and Ru, but negative ones for Tc, Mo, Nb, ...

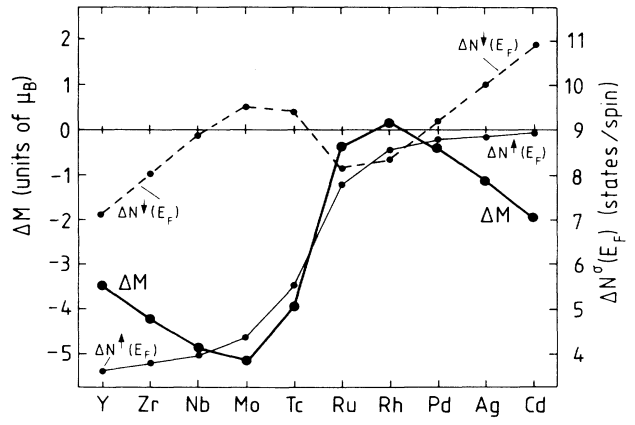

FIG. 7. Change $\Delta N^{\sigma}(E_F)$ of the majority ($\uparrow$) and minority ($\downarrow$) band populations for 4*d* impurities in Ni. $\Delta M = \Delta N^{\uparrow}(E_F) - \Delta N^{\downarrow}(E_F)$ is the change of the total moment.

The LDOS of all 4*d* impurities are characterized by a two-peak structure.[14] Owing to the strong hybridization with the host 3*d* electrons two peaks are splitting off from the upper and lower band edges, yielding similar LDOS for both spin directions. Since for Rh and even more for Ru the upper peak in the majority band has strong unoccupied tails above E_F, the criterium for strong ferromagnetism cannot be satisfied. In the 4*d* series one should have $\Delta N^{\uparrow}(E_F)=9$ in order to accomplish the criterium for strong ferromagnetism, since Pd has 18 more electrons than Ni. Instead we obtain only $\Delta N^{\uparrow}(E_F)=8.6$ for Rh and $\Delta N^{\uparrow}(E_F)=7.8$ for Ru. For Tc, being isoelectronic to Mn, we see already all signs of weak ferromagnetism: $\Delta N^{\uparrow}(E_F)$ is off by -3.5 from the "ideal" value of 9 and the moment ΔM is strongly negative ($\Delta M = -3.9\mu_B$). This is a direct consequence of the stronger hybridization: For Mn the virtual bound state in the majority band is rather narrow and squeezed into the region between the upper majority band and the Fermi energy, thereby being practically fully occupied. On the other hand, for Tc, this peak is much broader and therefore mostly empty.

The behavior of the early 4*d* impurities (Mo, Nb, Zr, Y) is similar to their 3*d* counterparts. $\Delta N^{\uparrow}(E_F)$ is nearly equal to $9-5=4$ and $\Delta N^{\downarrow}(E_F)$ decreases linearly with decreasing valence. The detailed discussion of Sec. II A therefore also applies here.

The experimental information about 4*d* impurities in Ni seems to be on shaky grounds. A detailed discussion can be found in Ref. 14. The situation is best for *Ni*Pd where the measurements of Sadron,[11] Crangle and Parson,[26] and Cable and Child[27] show a magnetization change of $\Delta M = 0 \pm 0.1\mu_B$, a very small local moment and practically no perturbation of the neighboring atoms. For *Ni*Rh the magnetization data[26,28] and the neutron scattering experiments show[29,30] unusual concentration dependence. Whereas the measurements for the dilute alloys point to $\Delta M \approx 2\mu_B$ and a local moment of $2\mu_B$ for Rh in contradiction to our calculation, the values extrapolated from higher concentrations would lead to $\Delta M \approx 0\mu_B$ and a local moment of $0.6-0.7\mu_B$. For *Ni*Ru two values for the local moment have been reported, $-3.1\mu_B$ by Madhav Rao *et al.*[31] and $0.2\mu_B$ by Parette and Kajzar[32] together with $\Delta M = -4.6\mu_B$. For *Ni*Mo Sadron[11] reports $\Delta M = -4.5\mu_B$.

In view of the good agreement between our results and the experiments for 3*d* impurities we believe that our calculations are of similar quality also for 4*d* impurities. A possible source of error could be the neglect of lattice relaxations in our calculations which are somewhat larger in the 4*d* series. However we do not believe that they would affect the results very much. It would therefore be good,

if especially the experiments for Rh and Ru could be repeated.

D. *sp* impurities in Ni

Table I lists the charge and magnetization perturbations in the four shells around the impurity. There is a considerable charge transfer from the impurity to the nearest neighbors especially for Ga, Ge, and As. Nevertheless the charge transfer is typically less than 10% of the valence difference ΔZ. Therefore it is clear that the rigid-band model requiring a charge transfer ΔZ is unrealistic. The screening is practically completed in the first shell so that longer-ranged charge perturbations are not important.

There is a rather small induced moment on the impurity site, which changes from negative to positive at the end of the series. Its origin has been explained by Katayama-Yoshida *et al.*[33] In short, the impurity *sp* states hybridize stronger with the host minority *d* states than with the majority ones, since the latter are more localized. The bonding hybrids which are the only states occupied for the early *sp* impurities have a stronger *sp* admixture for the minority spin direction and therefore the induced moment is negative. For the late *sp* impurities such as Se and Br the occupation of antibonding states in the majority band gives an important positive contribution, so that the local moment changes sign. This change is directly reflected in the impurity hyperfine field which also changes from negative to positive in the *sp* series. Similar to the observation for the early transition-metal impurities there is a strong reduction of the moments on the neighboring atoms and a weaker reduction for the atoms in the second, third, and fourth shell. Contrary to the charge changes there are no indications of oscillations for the magnetization. The only available neutron scattering data are for *Ni*Cu and give a reduction of the first neighboring Ni moment by $0.033\pm0.002\mu_B$ per atom,[34] which is exactly our calculated value. With increasing valence the magnetization disturbance increases. Especially the total change ΔM (Fig. 1) is well proportional to ΔZ for Cu, Zn, Ga, as well as Ag and Cd in the 5 *sp* series (Table III). For larger valences the moment change saturates at a value of about $-3\mu_B$ for Ge, As, and Se, in order to decrease again for Br and Kr (not calculated). Figure 2 shows the changes of the band population for both spin directions. For Cu, Zn, and Ga the majority population is unchanged and the additional charge is gained by filling up the minority band leading to the decrease of the moment $\Delta M=-\Delta Z$. For Ge, As, and Se additional electrons are added to both bands so that the moment saturates.

Terakura and Kanamori[13] have given a beautiful explanation of this apparent band filling process. For the early *sp* impurities like Cu, Zn, and Ga the atomic *s* and *p* levels of the impurity are located in energy appreciably above the Ni *d* band. Upon hybridization bonding and antibonding hybrids are formed. The energies of the bonding state emerge from the Ni *d* band and move to lower energies, whereas the antibonding states result from shifting the impurity *sp* states to higher energies. As far as the number of states is concerned there is a close correspondence between the hybridized states and the unhybridized ones. For instance there is a single degenerate antibonding state at higher energies, being *s*-like at the impurity site and having *d* admixtures at the neighboring sites, and a threefold degenerate "*p*-like" antibonding state. Moreover at lower energies the number of bonding states is the same as in the *d* band of elemental Ni. There is a slight complication due to the fact the *sp* impurities Cu, Zn, Ga, . . . have also occupied *d* states. However, this only means that we have to start with the *d*-*d* hybridized states of Ni with a Cu impurity, the number of which is exactly the same as the number of *d* states of pure Ni, and then hybridize these states with the impurity *s* and *p* states. The most important observation is that for the early *sp* impurities the antibonding states are high above E_F and cannot be occupied. Therefore the additional ΔZ electrons needed for charge neutrality can only be gained by populating more Ni *d* states, i.e., shifting the minority band of the nearest neighbors to lower energies, thus locally decreasing the Ni moments. The total change of the magnetization has to be exactly $\Delta M=-\Delta Z$, which is indeed found experimentally and in our calculations. Thus the old rigid-band model is correct as far as the state filling is concerned, but is totally wrong with respect to the local screening behavior. Moreover there is a new *sp* state above the Fermi energy, which one would not expect in the rigid-band model. Also the *d* band itself changes its form due to band narrowing, as we will discuss below. The bonding orbitals have strong *sp* admixtures at the impurity site and only the small charge transfer to the nearest neighbors shows that these orbitals are somewhat more Ni like.

For the later *sp* impurities the atomic *s* and *p* levels move down and we therefore also expect to occupy a new "*sp*-like" state introduced by the impurity. As seen in Fig. 2 this leads to an increase of the population in the majority band, e.g., for Ge, As, and Se, and the change in the minority band levels off, so that the moment ΔM saturates and decreases at the end of the series. The transition between these two screening processes, i.e., host *d*-state filling versus impurity *sp*-state filling is very smooth, contrary to the rather sudden transitions found in the 3*d* and 4*d* series.

The following figures (Figs. 8–12) give a somewhat more detailed description of the screening process. Figure 8 shows the symmetry decomposition of the changes $\Delta N^{\uparrow}(E_F)$ and $\Delta N^{\downarrow}(E_F)$, i.e., the decomposition into contributions from the different irreducible subspaces of the O_h group. The change $\Delta N^{\uparrow}(E_F)$ in the majority band is practically only due to Γ_1 and Γ_{15} contributions. Since these are the only subspaces which can couple to *s* states (Γ_1) and *p* states (Γ_{15}) at the impurity site, it is clear that the new states should appear only in these representations. All other contributions are negligible. The minority change $\Delta N^{\downarrow}(E_F)$ is for the early *sp* impurities mainly determined by the changes in the Γ_{12} and $\Gamma_{25'}$ representations. These are the subspaces which can couple to e_g-like states (Γ_{12}) and t_{2g}-like states ($\Gamma_{25'}$) at the impurity site. Since, e.g., for Zn and Ga there are no *d* states on the impurity site within the energy range of the Ni *d* band, those *d* states on the neighboring Ni sites which project to the Γ_{12} and $\Gamma_{25'}$ representations show a band narrowing,

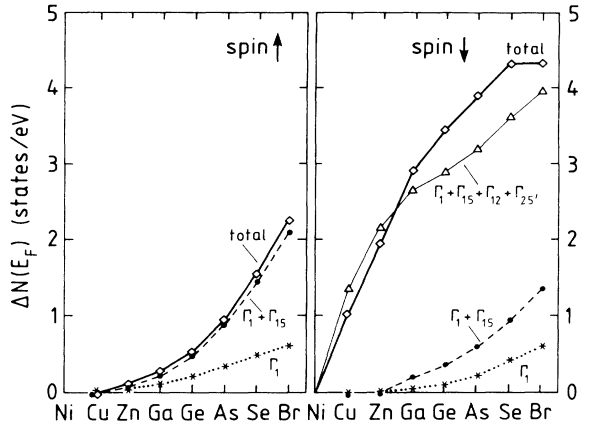

FIG. 8. Symmetry decomposition of $\Delta N^{\sigma}(E_F)$ into the irreducible representations of the O_h group. The representations Γ_1, Γ_{15}, Γ_{12}, and $\Gamma_{25'}$ transform such as s, p, d_{e_g}, and $d_{t_{2g}}$ orbitals at the impurity site.

thereby increasing the population in the minority band. Also here the *sp*-state filling occurs mostly in the Γ_1 and Γ_{15} representations. The contributions from all other representations are small, but in total not negligible. For instance, due to the reduction of the exchange splitting also the *d* population in other subspaces can increase. In total we see from Fig. 8 that both state-filling processes are strongly symmetry dependent, with the host *d*-state filling occurring mostly in the Γ_{12} and $\Gamma_{25'}$ subspaces and the impurity *sp* state filling in the Γ_1 and Γ_{15} subspaces.

As a representative example of the screening process by host *d* states we show in Figs. 9 and 10 the densities of states of Ga in Ni. Figure 9 shows the LDOS of the Ga impurity, i.e., the total LDOS and the partial *s* contribution. The difference between both curves is mostly of *p* character. The *s* and *p* bonding contributions are separated from the antibonding ones by a hybridization

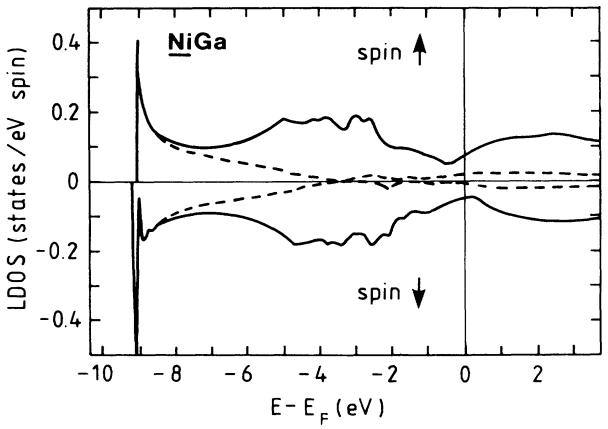

FIG. 9. LDOS (solid line) and partial *s*-LDOS (dashed line) of a Ga impurity in Ni.

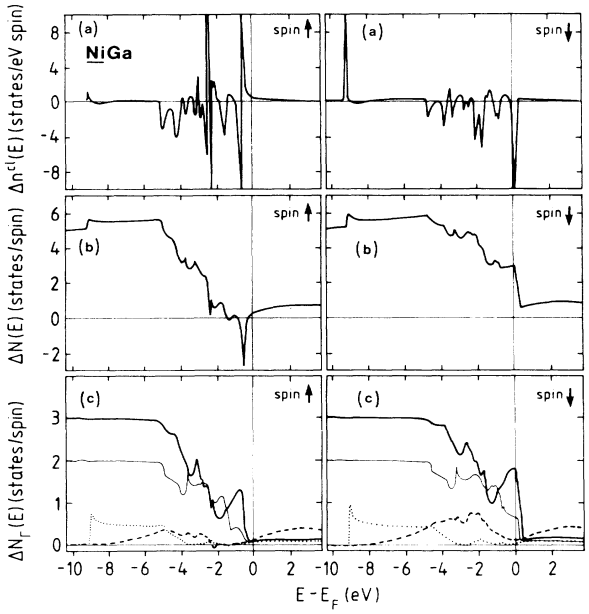

FIG. 10. (a) Change $\Delta n^{cl}(E)$ of the cluster DOS, (b) integrated total change $\Delta N(E)$ of the DOS, and (c) individual contributions $\Delta N_\Gamma(E)$ from different irreducible representations (Γ_1, Γ_{15}, Γ_{12}, and $\Gamma_{25'}$) of the O_h group for a Ga impurity in Ni.

minimum ["Fano resonance" (Ref. 35)] within the *d* band thus clearly separating the two different kinds of states responsible for the screening. Figure 10(a) shows the change $\Delta n^{cl}(E)$ of the density of states within the 55-atom cluster, whereas Fig. 10(b) shows the change of the integrated density of states. Since Ga has occupied 3*d* states at lower energies, $\Delta N(E)$ starts at -10 eV with a value of 5 for the five added *d* states for each spin direction. The subsequent increase is due to the filling of the bonding *s* and *p* states, which is in the *d*-band range followed by a depletion of *d* charge. At E_F we obtain practically no change in the majority band ($\Delta N^{\uparrow} \cong 0$) but $\Delta N^{\downarrow}(E_F) \cong 3$ due to the filling of the minority band. Fig-

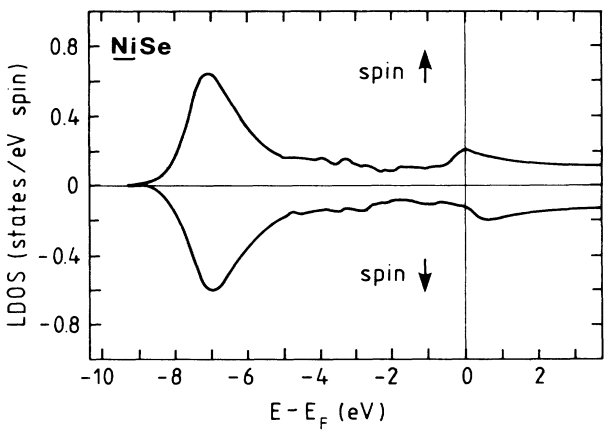

FIG. 11. LDOS of a Se impurity in Ni.

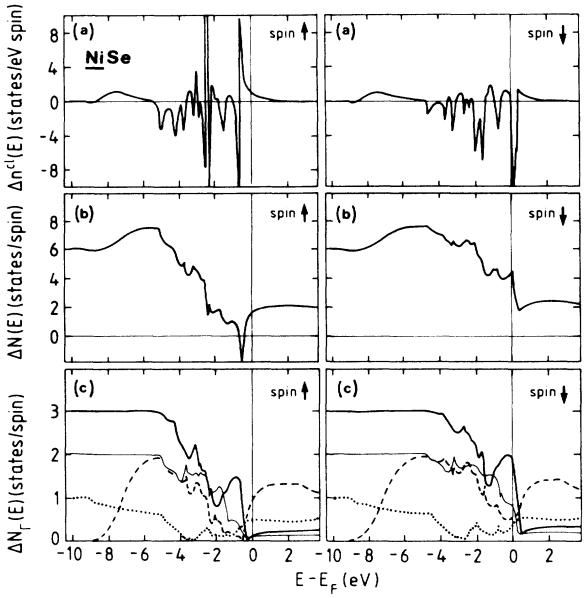

FIG. 12. (a) Change $\Delta n^{cl}(E)$ of the cluster DOS, (b) integrated total change $\Delta N(E)$ of the DOS, and (c) individual contributions $\Delta N_\Gamma(E)$ from the Γ_1, Γ_{15}, Γ_{12}, and $\Gamma_{25'}$ representations for a Se impurity in Ni.

ure 10 show the contributions $\Delta N_\Gamma(E)$ from the four representations Γ_1, Γ_{15}, Γ_{12}, and $\Gamma_{25'}$ of O_h group. Here it is most important that the minority band filling occurs in the Γ_{12} and $\Gamma_{25'}$ representations.

Figures 11 and 12 show the corresponding results for Se in Ni for which according to Figs. 2 and 8 the *sp*-state filling mechanism is quite important. The LDOS of Se shows strong-bonding *p* peaks at about -7 eV and weak antibonding *p* peaks close to E_F. The *s* intensities are rather small, since the 4*s* state is localized below the band (at -14.2 eV). The changes $\Delta n^{cl}(E)$ and $\Delta N(E)$ are very similar to the ones of Ga. Owing to the additional bound *s* state we start with a value of 6 for $\Delta N^\uparrow$ and $\Delta N^\downarrow$ at lower energies. The *s*-like integrated density of states (DOS) $\Delta N_{\Gamma_1}(E)$ starts at -10 eV with a value of 1, continuously decreases due to antiscreening to about 0 at the hybridization minimum at about -3 eV and then increases due to the population of antibonding states. An analogous behavior is also found for the *p*-like DOS $\Delta N_{\Gamma_{15}}(E)$, only that the *p* state is not yet localized and that the hybridization minimum is higher in energy. Thus the addition of new states arises due to the population of the antibonding states and not due to the population of new impurity *s* and *p* states deep below E_F. Since in the majority band these states are somewhat lower in energy than in the minority band this effect leads to an important positive magnetization contribution to ΔM as well as to the positive polarization and positive hyperfine field of the impurity. In total however the magnetization change ΔM is negative due to the large Γ_{12} and $\Gamma_{25'}$ contributions in the minority band.

IV. SUMMARY AND CONCLUSIONS

We have performed extensive *ab initio* calculations for 3*d*, 4*d*, and 4*sp* impurities in Ni and have calculated self-consistently the charge and magnetization perturbations for four shells around the impurities. For the 3*d* series the calculations are in agreement with and confirm the tight-binding model calculations of Friedel,[3] Kanamori,[4] and Campbell and Gomes.[5] We find *Ni*Co and *Ni*Fe to be strong ferromagnets, while *Ni*Mn is on the verge of becoming weak. The early 3*d* impurities couple antiferromagnetically to the host moment and induce a large magnetization reduction on the neighboring shells. The early 4*d* impurities show a very similar behavior. However Ru, Rh, and Pd are unique since these alloys are neither strong nor weak ferromagnets. In agreement with the discussion of Terakura and Kanamori[13] we find that the early *sp* impurities are screened by host minority *d* states whereas for the late *sp* impurities new impurity states in the form of antibonding states are populated close to the Fermi energy and provide part of the screening. For the 3*d* and 4*sp* impurities the calculated change ΔM of the total moment and the calculated magnetization perturbations are in good agreement with the experimental data. Some discrepancies exist however for 4*d* impurities, especially for Ru and Rh. Here more experimental work is desirable to clear up these problems.

ACKNOWLEDGMENT

We thank Dr. H. Akai for helpful discussions.

[1] S. Chikazumi, *Physics of Magnetism* (Wiley, New York, 1964), p. 73.
[2] A. R. Williams, V. L. Moruzzi, A. P. Malozemoff, and K. Terakura, IEEE Trans. Magn. **MAG-19**, 1983 (1983); A. P. Malozemoff, A. R. Williams, K. Terakura, V. L. Moruzzi, and K. Fukamichi, J. Magn. Magn. Mater. **35**, 192 (1983).
[3] J. Friedel, Nuovo Cimento **10**, Suppl. No. 2, 287 (1958).
[4] J. Kanamori, J. Appl. Phys. **16**, 929 (1965).
[5] I. A. Campbell and A. A. Gomes, Proc. Phys. Soc., London **91**, 319 (1967).
[6] G. G. Low, Adv. Phys. **18**, 371 (1969).
[7] A. P. Malozemoff, A. R. Williams, and V. L. Moruzzi, Phys. Rev. B **29**, 1620 (1984).
[8] A. R. Williams, A. P. Malozemoff, V. L. Moruzzi, and M. Matsui, J. Appl. Phys. **55**, 2353 (1984).
[9] R. P. Messmer, Phys. Rev. B **23**, 1616 (1981).
[10] B. W. Corb, R. C. O'Handley, and N. J. Grant, Phys. Rev. B **27**, 636 (1983).
[11] C. Sadron, Ann. Phys. (Paris) **17**, 371 (1932).
[12] J. Crangle and M. J. C. Martin, Philos. Mag. **4**, 1006 (1959).
[13] K. Terakura and J. Kanamori, Prog. Theor. Phys. **46**, 1007 (1971); K. Terakura, J. Phys. F **6**, 1385 (1976).

[14]R. Zeller (unpublished).
[15]S. Blügel, H. Akai, R. Zeller, and P. H. Dederichs, Phys. Rev. B **35**, 3271 (1987).
[16]R. Podloucky, R. Zeller, and P. H. Dederichs, Phys. Rev. B **22**, 5777 (1980).
[17]P. J. Braspenning, R. Zeller, A. Lodder, and P. H. Dederichs, Phys. Rev. B **29**, 703 (1984).
[18]V. von Barth and L. Hedin, J. Phys. C **5**, 1629 (1972); V. L. Moruzzi, J. F. Janak, and A. R. Williams, *Calculated Electronic Properties of Metals* (Pergamon, New York, 1978).
[19]R. Zeller, J. Deutz, and P. H. Dederichs, Solid State Commun. **44**, 993 (1982).
[20]H. Akai and P. H. Dederichs, J. Phys. C **18**, 2455 (1985).
[21]G. Lehmann, Phys. Status Solidi B **70**, 737 (1975); P. Lloyd, Proc. Phys. Soc., London **90**, 207 (1967).
[22]A. J. P. Meyer and G. Asch, J. Appl. Phys. **32**, 3305 (1961).
[23]F. Kajzar and G. Parette, J. Magn. Magn. Mater. **15-18**, 87 (1980).
[24]F. Livet and P. Radhakrisna, J. Phys. Chem. Solids **38**, 275 (1977).
[25]J. W. Cable and R. A. Medina, Phys. Rev. B **13**, 4868 (1976).
[26]J. Crangle and D. Parsons, Proc. R. Soc. London, Ser. A **255**, 509 (1960).
[27]J. W. Cable and H. R. Child, Phys. Rev. B **1**, 3809 (1970).
[28]W. C. Mueller and J. S. Kouvel, Phys. Rev. B **11**, 4552 (1975).
[29]J. W. Cable, Phys. Rev. B **15**, 3477 (1977).
[30]J. W. Cable and E. O. Wollan, Physica **86-88B**, 745 (1977).
[31]L. Madhav Rao, R. Chakravarthy, Z. Jirak, and N. S. Satya Murthy, Phys. Rev. B **18**, 6275 (1978).
[32]G. Parette and F. Kajzar, J. Phys. F **9**, 1867 (1979).
[33]H. Katayama-Yoshida, K. Terakura, and J. Kanamori, J. Phys. Soc. Jpn. **46**, 822 (1979); **48**, 1504 (1980); **49**, 972 (1980); J. Kanamori, H. Katayama-Yoshida, and K. Terakura, Hyperfine Interact. **8**, 573 (1981).
[34]A. T. Aldred, B. D. Rainford, T. J. Hicks, and J. S. Kouvel, Phys. Rev. B **7**, 218 (1973).
[35]K. Terakura, J. Phys. F **7**, 1773 (1977).